

A nonlinear stability analysis of aircraft controller characteristics outside the standard flight envelope

STEPHEN J. GILL, MARK H. LOWENBERG AND SIMON A. NEILD
Faculty of Engineering, University of Bristol, Bristol, BS8 1TR, UK

LUIS G. CRESPO
National Institute of Aerospace, 100 Exploration Way,
Hampton VA 23666 USA

BERND KRAUSKOPF
Department of Mathematics, University of Auckland,
Private Bag 92019, Auckland 1142, New Zealand

GUILHEM PUYOU
Airbus France, 31060 Toulouse Cedex 03, France

August 2014

Abstract

In this paper we evaluate the influence of the flight control system over the off-nominal flying dynamics of a remotely operated air vehicle. Of particular interest is the departure/upset behaviour of the closed-loop system near stall. The study vehicle is the NASA Generic Transport Model and both fixed-gain and gain-scheduled versions of a LQR-PI controller are evaluated. The differences in effectiveness of the controllers are first demonstrated with time responses to fixed commands. Then, bifurcation analysis is used to characterize spiral and spin behaviour of the aircraft in both open- and closed-loop configurations. This yields an understanding of the underlying vehicle dynamics outside the standard flight envelope, hence it provides a means of assessing the effectiveness of the controller and evaluating the upset tendencies of the aircraft.

1 Introduction

The use of feedback control systems in civil aircraft is well established, with relatively complex control laws in place on modern fly-by-wire airliners; see [1] for example. These are designed for nominal flight conditions where the aircraft is close to symmetric trimmed or manoeuvring flight, and incorporate envelope-limiting functions to attempt to prevent excursions beyond the nominal flight envelope. The control law design process typically utilises linear methods, often based on linear time-invariant (LTI) models, even if the final controller is nonlinear by virtue of scheduling between gains designed at specific operating points.

Despite such control laws, that aim to maintain a safe operating envelope, the problem of airliners encountering upset phenomena leading to loss-of-control (LOC) does exist [2]. This is characterised by a flight trajectory involving large deviations in attitude and angular rates. During such excursions, the aircraft dynamics are dominated by aerodynamic forces and torques that are strongly nonlinear and might be coupled with the moments of inertia and pilot commands. It is often of interest to determine if the flight controller plays a beneficial role on the recovery from vehicle upsets. Generally, LTI models are, however, of limited value when analysing nonlinear systems. Unfortunately, most of the mathematical tools for control analysis are based on such models [3].

A variety of control design approaches have been developed to overcome the limitations of linear controllers. A popular approach is gain-scheduling, where a set of linear controllers are designed at several operating points and then blended together with respect to an input or state variable [4]. They do, however, usually suffer the limitation of being designed only at trim points within the expected operating envelope and, hence, may not cope well with nonlinearity under off-nominal conditions. Also, care needs to be exercised when scheduling with respect to a state variable that changes rapidly. To overcome the limitations of linearity, much work has been done on nonlinear control law design, such as by dynamic inversion [5] and a host of adaptive techniques [6, 7]. These are also not necessarily problem-free, with issues such as robustness to model uncertainty and stability guarantees requiring special attention. Typically, nonlinear controllers are also evaluated only under nominal operating conditions (i.e. those within the expected operating range, and up to the stall), partly because this is how the design requirements are stipulated.

Whether implementing gain-scheduled control or another nonlinear approach, a suitably representative mathematical model is needed. Due to the increased nonlinearity and time-dependence inherent in flight dynamics behaviour under off-nominal conditions – particularly at high angles of attack and/or sideslip – such models are more difficult and expensive to create than conventional models and will inevitably incorporate far higher levels of uncertainty. Hence, they do not generally exist for civil aircraft. However, researchers at NASA Langley have created the Generic Transport Model (GTM): this represents a dynamically scaled version of a twin-engine jet vehicle with a geometry characteristic of low-wing airliners with under-wing-mounted engines [8]. The purpose of the model, derived from a comprehensive wind tunnel test campaign as well as from remotely piloted tests of a powered flight vehicle, was indeed to generate a representative wide-envelope airliner flight dynamics model for the simulation and analysis of upset and LOC [9]. A similar model was created for the EU ‘Simulation of UPset Recovery in Aviation’ (SUPRA) research programme [10].

To gain insight into the behaviour of a nonlinear dynamical model, it is necessary to understand its ‘structure’: its multiple steady state solution branches, their stability and changes thereof (at bifurcation points) and the dependence of these structures on parameter variations. Whilst the generation of time history simulations from such models is useful, it provides very limited information on the above. Numerical bifurcation analysis, on the other hand, implemented via continuation algorithms [11], has been shown to be extremely useful in facilitating an understanding of solution characteristics in state-parameter space, allowing response types to be inferred not only locally but also ‘globally’ across a wide operating region [12].

One field in which continuation and bifurcation analysis has indeed demonstrated significant value is that of nonlinear flight dynamics of aircraft. Since the earliest applications, for example in Carroll and Mehra [13], Guicheteau [14] and Zagaynov and Goman [15], it has been applied to a number of military aircraft models, showing the development of phenomena such as wing rock, inertial coupling and spins (e.g. [16]) and the influence of highly augmented control systems (e.g. [17]). Ref. [18] provides a comprehensive survey of bifurcation analysis applied to fixed-wing flight dynamics problems. This approach has recently been implemented on the NASA Generic Transport Model (GTM) [12] and the SUPRA model [10] in open-loop form, and has revealed spiral dives and steep spins. An early extension of the approach to closed-loop controllers deployed bifurcation analysis to assess the stability of a wing rock controller with different gains [19]. Bifurcation analysis of closed-loop aircraft has primarily been used to analyse control laws; then the bifurcation diagrams were used to help design control schemes to improve the aircraft behaviour. Littleboy and Smith [20] used bifurcation analysis to analyse open-loop and then closed-loop versions of the ‘Hypothetical High-Incidence Research Model’ to contribute to control law design through nonlinear dynamic inversion.

Jones et al. [21] developed the idea of dynamic gain-scheduling where the controller gains were designed as parameters varied within a continuation routine. Here, for each continuation step the trim point is calculated and gains designed by means of a linear quadratic regulator (LQR). This defines a gain schedule with a superior resolution, which is then transformed such that, when scheduled with a fast-varying state, the intended local stability remains valid. However, this method only concerns the aircraft in trim settings and does not assure that off-nominal flight conditions have been stabilised. Bifurcation analysis of the NASA GTM aircraft coupled to a linear parameter varying (LPV) control system was performed by Kwatny et al. [22]. This used bifurcation analysis to perform a rigorous examination of control and regulation around the stall point and showed how controllability is lost at bifurcation points; it also defined safe sets for the aircraft operation and considered recovery from upset in the presence of damage. However, whilst the dynamics of the closed-loop GTM around the stall point was within the scope of this study, controller effects in other off-nominal conditions were not.

A note in [19] mentions how continuation methods can be used to help tuning the control law. This

idea is extended by Goman and Khrantsovsky [23] who also analysed a controller designed to suppress wing rock. Here, a two-parameter bifurcation diagram was used to show the combinations of gains for which the controller eliminated wing rock. However, these wing rock controllers use only simple proportional feedback which, although successful for the suppression of wing rock, are not fully representative of controllers typically used on civil transport aircraft. Richardson et al. [24] extended this idea of continuing controller gains by use of a scalar ‘gain parameter’ which is applied to the state-feedback gains in a feedback-plus-feedforward gain-scheduled controller designed to meet handling qualities objectives by using eigenstructure assignment: it effectively varies a selection of gains simultaneously between zero (when the gain parameter is zero) and their design values (gain parameter unity) and beyond (gain parameter > 1). This study showed that, whilst desired handling qualities were achieved under nominal operating conditions, an undesirable isola that adversely affects system response was identified; it disappeared only when the gain parameter exceeded one. This illustrates the power of numerical continuation when used to inform controller design. Although integral control was applied to this system, the gain parameter continuation was applied only to the proportional gains, and was therefore relatively simple in nature.

This paper extends the bifurcation analysis performed in [12] to analyse the dynamics of the GTM; it builds on the approach of Richardson et al. [24] to explore the means by which continuation methods can yield a deeper insight into the influence of control laws on the nonlinear system behaviour. Design of these control laws is described in [25], and here analysis of both fixed gain and gain scheduled versions of the controller is undertaken. The mathematical model of the closed-loop GTM consists of an airframe dynamics model – featuring aerodynamic, inertial, kinematic and control surface position and rate saturation nonlinearities – and a flight control system. The latter consists of (i) a longitudinal controller having the elevator deflections as control input, (ii) an auto-throttle having the throttle-input to both engines as control input, and (iii) a lateral/directional multivariable controller having the ailerons and rudders as inputs. These controllers, which assume a full-state feedback feedforward structure, define the control law. The feedforward component of the controller is driven by commands generated by the pilot. These commands, which are exogenous signals to the system, are created by the pilot based on the aircraft’s current state and the desired steady-state flight condition.

The paper is organized as follows. In Section II the aircraft model and controller architecture are described and their performance briefly compared using time responses. In Section III the bifurcation analysis of the open-loop GTM is summarised, with an emphasis on upset behaviour; an assessment is then made of the changes in the system attractors as the control loop is closed, focusing on the spiral and spin solutions and their respective stability characteristics. Finally, in Section IV, conclusions are drawn concerning the changes in off-nominal attractors arising from using a control law, hence, the benefits offered by bifurcation methods in evaluating closed-loop flight dynamics.

2 Plant and Controller Architecture

2.1 The Generic Transport Model

The GTM is a model of a commercial transport aircraft for which both a dynamically scaled flight test vehicle and a high-fidelity simulation model were developed. Figure 1 shows the flight test vehicle and its concept of operation. References [26, 8, 27] provide details on the vehicle’s configuration and characteristics and the flight experiments. The aircraft is piloted from a ground station via radio frequency links by using onboard cameras and synthetic vision technology. The high-fidelity simulation model, known as the DesignSim, uses nonlinear aerodynamic models extracted from wind tunnel data and system identification for conditions that include high angles of attack, and considers actuator dynamics with rate and range limits, engine dynamics, sensor dynamics along with analog-digital-analog latencies and quantization, sensor noise and biases, telemetry uplink and downlink time delays, turbulence, atmospheric conditions, etc. The open-loop system model has 278 state variables.

During stall, which occurs between angles of attack of 12° and 14° degrees, the vehicle experiences a drop in altitude and an uncommanded roll departure. These effects, which are captured by the aerodynamic model of the DesignSim, mimic the behaviour of the test article observed in the flight experiments. A high level description of the flight controllers used for in the bifurcation analysis is presented next. For additional details on the development of these controllers, see [7].



Figure 1: NASA GTM test article and its concept of operations [7].

2.2 Control Design

The system dynamics can be represented as

$$\dot{X} = F(X, U), \quad (1)$$

where F is a nonlinear function of the state vector X and the control input U . For control design purposes, this nonlinear plant is linearized about a trim point (X^*, U^*) satisfying $F(X^*, U^*) = 0$ for the force and moment equations. Deviations from the trim values X^* and U^* are written as lower-case letters hereafter, e.g., $X = X^* + x_p$ and $U = U^* + u$. Linearization of Eq. (1) about the trim point leads to the system

$$\dot{x}_p = A_p x_p + B_p u + \nu(x_p, u), \quad (2)$$

where

$$A_p = \left. \frac{\partial F}{\partial X} \right|_{X^*, U^*} \quad B_p = \left. \frac{\partial F}{\partial U} \right|_{X^*, U^*} \quad (3)$$

and ν contains higher-order terms. In a sufficiently small neighbourhood of the trim point, the effect of the higher-order terms is negligible. The LTI representation of the plant, which results from dropping the higher-order terms from Eq. (2), is given by

$$\dot{x}_p = A_p x_p + B_p (R_s(u) + d) + B_2 \hat{r}, \quad (4)$$

where A_p and B_p are the system and control input matrices, $d(t)$ is an exogenous disturbance; $\hat{r}(t)$ is the reference command generated by the pilot; $R_s(u)$ is a saturation function that enforces range saturation limits in the control inputs, and B_2 is the command input matrix.

The state, x_p , consists of angle of attack, α ; sideslip angle, β ; speed, V ; roll rate, p ; pitch rate, q ; yaw rate, r ; longitude, x ; latitude, y ; altitude, z ; and the Euler angles, ψ , θ , and ϕ . The control input u consists of the elevator deflection, δ_e ; the aileron deflection, δ_a ; the rudder deflection, δ_r ; and the throttle input to the engines, δ_{th} . The reference command \hat{r} consists of angle of attack-, sideslip-, speed- and roll rate-commands. These four commands, denoted hereafter as α_{cmd} , β_{cmd} , V_{cmd} , and p_{cmd} , respectively, are generated by the pilot to attain the desired flight manoeuvre.

The flight controller consists of independent controllers for the longitudinal and the lateral/directional dynamics. While the longitudinal controller consists of an auto-throttle and a multiple-input-single-output controller for pitch, the lateral/directional controller assumes a multiple-input-multiple-output structure. The controllers operating the control surfaces have a linear quadratic regulator structure with proportional and integral (LQR-PI) terms having integral error states for each of the components of the reference command \hat{r} . Furthermore, strategies for preventing integrator windup caused by input saturation were applied [7]. A fixed control allocation matrix that correlates inputs of the same class prescribes the 10 main plant inputs: 4 elevators, 2 ailerons, 2 rudders and 2 throttles. As a result, out of these 10 inputs only 4 are independent.

2.2.1 Auto-throttle

The throttle input to the engines was prescribed by a simple proportional-derivative controller with the form

$$\delta_{th} = K_1 e_V + K_2 \dot{e}_V, \quad (5)$$

where

$$e_V = V - V_{\text{cmd}}. \quad (6)$$

The regulation of airspeed and pitch control were done separately because of a large time scale separation between the corresponding actuators. In a previous work [7], a multivariable controller for both airspeed and pitch was developed.

2.2.2 Longitudinal Controller

The linearized plant for pitch control takes the form

$$\dot{x}_{\text{lon}} = A_{\text{lon}} x_{\text{lon}} + B_{\text{lon}} u_{\text{lon}}, \quad (7)$$

where $A_{\text{lon}} \in \mathbb{R}^{3 \times 3}$ is the system matrix, $B_{\text{lon}} \in \mathbb{R}^{3 \times 1}$ is the input matrix, $x_{\text{lon}} = [\alpha \ q \ V]^\top$ is the state, and $u_{\text{lon}} = \delta_e$ is the input. To enable tracking commands in angle of attack, the integral error state

$$e_\alpha = \int (\alpha - \alpha_{\text{cmd}}) dt, \quad (8)$$

was added. This led to the augmented plant

$$\begin{bmatrix} \dot{x}_{\text{lon}} \\ \dot{e}_\alpha \end{bmatrix} = \begin{bmatrix} A_{\text{lon}} & 0 \\ H_1 & 0 \end{bmatrix} \begin{bmatrix} x_{\text{lon}} \\ e_\alpha \end{bmatrix} + \begin{bmatrix} B_{\text{lon}} \\ 0 \end{bmatrix} \delta_e + \begin{bmatrix} 0 \\ -1 \end{bmatrix} \alpha_{\text{cmd}}, \quad (9)$$

where $H_1 = [1, 0, 0]$. A constant gain LQR controller that minimizes

$$J = \int_0^\infty (x_{\text{lon}}^T Q x_{\text{lon}} + \delta_e^2 R) dt, \quad (10)$$

where $Q = Q^\top \geq 0$, $R > 0$ are weighting matrices, was designed. This led to

$$\delta_e = [K_{\text{lon}} \ K_{e_\alpha}] \begin{bmatrix} x_{\text{lon}} \\ e_\alpha \end{bmatrix}. \quad (11)$$

This controller must attain ample stability margins so the low-pass- and anti-aliasing-filters from sensors and the delay caused by telemetry do not compromise stability.

The plant's input is given by

$$R_s(u) = \begin{cases} u & \text{if } u_{\min} < u < u_{\max}, \\ u_{\max} & \text{if } u \geq u_{\max}, \\ u_{\min} & \text{otherwise,} \end{cases} \quad (12)$$

where u is the controller's output, and u_{\max} and u_{\min} are the saturation limits of the actuator. The control deficiency caused by this saturation function is given by

$$u_\Delta = R_s(u) - u. \quad (13)$$

The integrator anti-windup strategy proposed in [7] is applied to the $\langle e_\alpha, \delta_e \rangle$ pair.

2.2.3 Lateral/Directional Controller

An LTI model of the corresponding plant is

$$\dot{x}_{\text{lat}} = A_{\text{lat}}x_{\text{lat}} + B_{\text{lat}}u_{\text{lat}}, \quad (14)$$

where $A_{\text{lat}} \in \mathbb{R}^{3 \times 3}$ is the system matrix, $B_{\text{lat}} \in \mathbb{R}^{3 \times 2}$ is the input matrix, $x_{\text{lat}} = [\beta \ p \ r]^\top$ is the state, and $u_{\text{lat}} = [\delta_a \ \delta_r]^\top$ is the input. To enable satisfactory command following, integral error states for sideslip and roll rate, given by

$$e_\beta = \int (\beta - \beta_{\text{cmd}}) dt, \quad (15)$$

$$e_p = \int (p - p_{\text{cmd}}) dt, \quad (16)$$

were added. The integral error in sideslip was chosen over that of the yaw rate to facilitate the generation of commands for coordinated turns with non-zero bank angles and cross-wind landing. The augmented plant is given by

$$\begin{bmatrix} \dot{x}_{\text{lat}} \\ \dot{e}_\beta \\ \dot{e}_p \end{bmatrix} = \begin{bmatrix} A_{\text{lat}} & 0 \\ H_2 & 0 \end{bmatrix} \begin{bmatrix} x_{\text{lat}} \\ e_\beta \\ e_p \end{bmatrix} + \begin{bmatrix} B_{\text{lat}} \\ 0 \end{bmatrix} u_{\text{lat}} + \begin{bmatrix} 0 \\ -I \end{bmatrix} \begin{bmatrix} \beta_{\text{cmd}} \\ p_{\text{cmd}} \end{bmatrix}, \quad (17)$$

where $H_2 = [[1, 0]^\top \ [0, 1]^\top \ [0, 0]^\top]$. A LQR control structure for the lateral controller was adopted. This led to

$$\begin{bmatrix} \delta_a \\ \delta_r \end{bmatrix} = [K_{\text{lat}} \ K_{e_\beta} \ K_{e_p}] \begin{bmatrix} x_{\text{lat}} \\ e_\beta \\ e_p \end{bmatrix}. \quad (18)$$

As before, this controller attains ample stability margins to accommodate for filters and time delays. The anti-windup technique in [7] is applied to the $\langle e_\beta, \delta_r \rangle$ and $\langle e_p, \delta_a \rangle$ pairs.

2.2.4 Control Allocation

Equations (5), (11) and (18) along with the three realizations of the anti-windup technique mentioned above, prescribe the preallocated input $u_n = [\delta_e \ \delta_a \ \delta_r \ \delta_{th}]^\top$, where

$$u_n = K_n [x_{\text{lon}} \ e_\alpha \ e_V \ \dot{e}_V \ x_{\text{lat}} \ e_\beta \ e_p]^\top, \quad (19)$$

and $K_n \in \mathbb{R}^{4 \times 11}$ is the feedback gain. This input, along with a control allocation scheme, fully determines the 10 control inputs of the aircraft. This relationship can be written as

$$u_{\text{nom}} = G_{\text{nom}} u_n, \quad (20)$$

where $G_{\text{nom}} \in \mathbb{R}^{10 \times 4}$ is the control allocation matrix. The allocation of u_n enforced by G_{nom} makes the four elevators deflect the same, both ailerons deflect in opposite directions, the thrust of both engines equal, and the deflection of both rudders equal.

2.3 Competing Control Alternatives

This section presents details of the development and configuration of the two flight control systems to be evaluated.

The open-loop longitudinal dynamics are unstable for angles of attack in the range 11.9°-12.8° while the lateral/directional dynamics are unstable in the 10.4°-14.25° and 23.85°-28.4° ranges. Stall occurs in the first of these three ranges. The non-zero aileron and rudder deflections necessary for trim are the result of minor asymmetries in the mounting of the engines, a slight offset between the centroid of the fuselage and the centre of gravity (c.g.) and asymmetry in the vehicle aerodynamics. The asymmetry resulting from the engine mounting is more noticeable at high angles of attack because its effects are proportional to the engine's thrust.

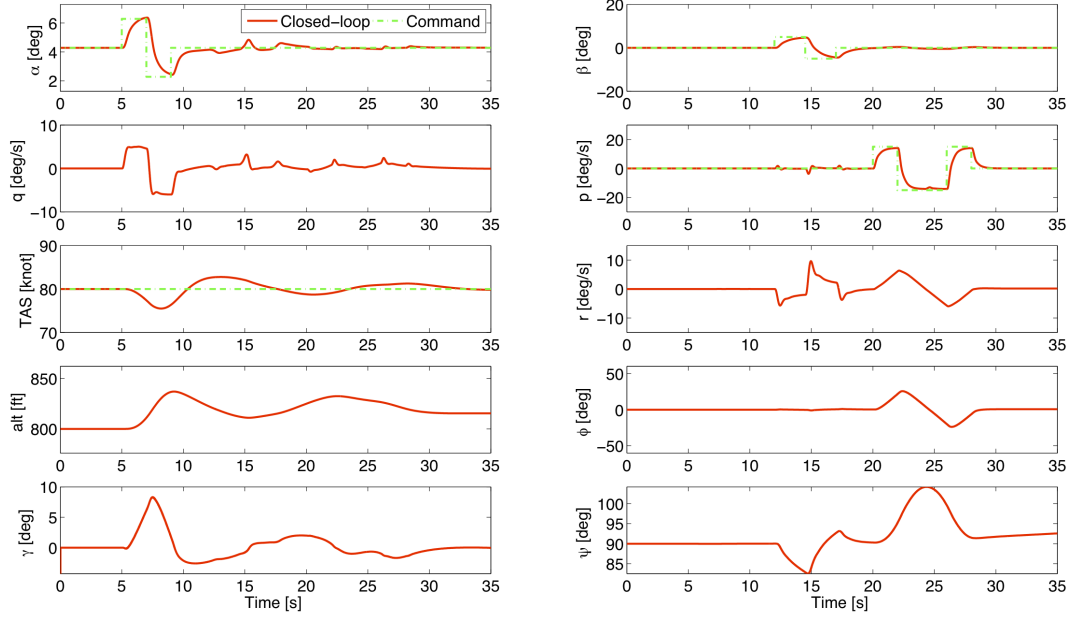


Figure 2: Aircraft states and commands corresponding to manoeuvres within the standard flight envelope for controller \mathcal{C}_1 .

A single-trim-point flight controller for X^* and U^* was designed first, for a horizontal wings-level flight condition and 80 knots ($41.2m/s$) air speed; the corresponding angle of attack is 4.28° and the flight path angle, γ , is zero. This controller consists of the auto-throttle, the longitudinal and the lateral/directional controllers introduced above. This controller will be denoted as \mathcal{C}_1 . The controller gains were tuned according to classical control metrics, which included stability margins, shaping of the input- and output-loop transfer-functions, and time responses to representative pilot commands. It is the fast modes of motion of the vehicle that are important in this process as the slower modes (in particular the spiral) can be compensated by either the pilot or an autopilot. The control objective was to obtain a controller that provides satisfactory pilot command tracking given the intrinsic time delays of the system.

Figure 2 shows the states and commands corresponding to a typical manoeuvre within the normal flight envelope. The aircraft starts off from the trim point used for control design and then it is subjected to commands in angle of attack, side-slip, and roll rate. It can be seen that the controller tracked the doublets well while reaching the commanded airspeed after a short transient without significant changes in altitude.

Figure 3 shows the same manoeuvre but for a sequence of commands centred about a trimmed point with a higher angle of attack. A substantial degradation in tracking performance occurs because this flight condition is far from the trim point X^* used in the control design. Note that appearance of uncommanded oscillations in pitch and the instabilities in both roll and yaw. Even though this controller attains good command tracking near 4.28° , it fails to locally stabilize the aircraft over the entire equilibrium manifold. Providing there is enough control authority, the aircraft might be kept near a locally unstable equilibrium point by a judicious and persistent set of commands \hat{r} .

To improve the command tracking performance outside the normal flight envelope, gain-scheduled controllers were designed [28]. One of these, denoted as \mathcal{C}_2 and which can be regarded as moderately aggressive in its tracking performance, is considered in this paper. This controller schedules three fixed-point controllers on the longitudinal and lateral axes with angle of attack. Since the scheduling variable is a state, the resulting controller is quasi-linear parameter varying. The trim points used for control design correspond to angles of attack of 4.28° , 13° , and 22° . These values correspond to cruise, stall, and post-stall flight conditions, respectively. Each of the fixed-point controllers comprising the gain scheduled controller attains good tracking performance near

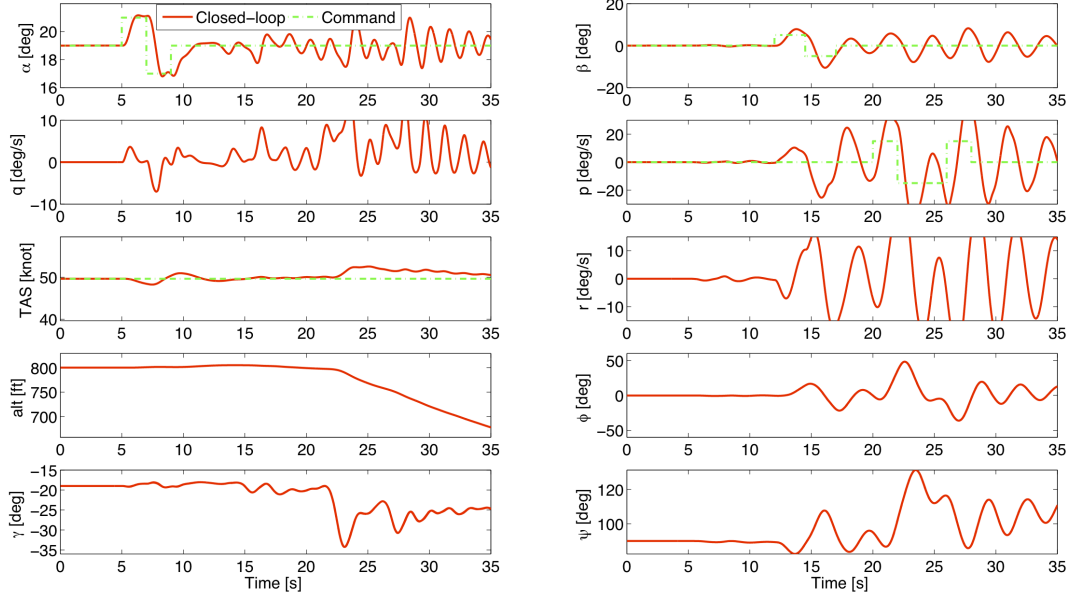


Figure 3: Aircraft states and commands corresponding to manoeuvres outside the standard flight envelope for controller \mathcal{C}_1 .

the corresponding linearization point. Furthermore, they make the important modes of the equilibrium manifold locally stable at each point in the 2° - 30° degree angle of attack range. The controller used by the gain scheduled controller at 4.28° is the very same \mathcal{C}_1 .

In contrast to the fixed-point controller, \mathcal{C}_1 , the gain-scheduled controller, \mathcal{C}_2 , attains a command tracking performance in all axes that is satisfactory and similar throughout the 2° - 28° degree range of angle of attack. For larger angles of attack, good V command tracking is no longer possible due to the reduced control authority resulting from the saturation of the throttle input.

3 Bifurcation Analysis









In this section we first summarize aspects of the multi-attractor dynamics underlying the open-loop behaviour of the GTM, by means of bifurcation diagrams. We then consider how these change when the loop is closed with the controllers \mathcal{C}_1 and \mathcal{C}_2 , with particular emphasis on off-nominal conditions and upset with the controller \mathcal{C}_1 . Upset is defined in the Upset Recovery Training Aid (URTA) [29] as an inadvertent event where:

- Pitch angle, θ , goes beyond the set $[-10^\circ, 25^\circ]$,
- Roll angle, ϕ , exceeds $\pm 45^\circ$,
- or flying with an inappropriate airspeed.

The other commonly used definition of upset is that by Lambregts et al. [30] where upset is an uncommanded or inadvertent event with an abnormal:

- attitude,
- rate of change of attitude,
- acceleration,
- airspeed, or
- with an inappropriate flight trajectory.

Table 1: Bifurcation diagram notation.

	Stable equilibrium		Hopf bifurcation
	Stable 6-state equilibrium		Torus bifurcation
	Unstable equilibrium		Period doubling bifurcation
	Stable periodic orbit		
	Unstable periodic orbit		

In this paper, these two often used definitions shall be used to assess which dynamics regimes uncovered by the bifurcation analysis represent upset conditions.

Results from numerical continuation applied to the GTM as described in Ref. [12] are presented here as one-parameter bifurcation diagrams; these indicate the dependence of steady state solutions of the dynamical system on the variation of a single parameter. In the open-loop case, the parameter in the diagrams shown here is elevator angle, whilst in the close-loop cases it is either the commanded angle of attack by the pilot α_{cmd} or a ‘gain parameter’ GP on the controller gains (defined in Section 3.2). α_{cmd} was chosen as the continuation parameter to allow comparison to the open-loop results. This is possible as the longitudinal controller turns an α_{cmd} input into an elevator deflection, hence, there is a direct link between α_{cmd} and δ_e in the closed-loop system. Local stability is indicated on the solution branches and is used, along with the topology of the diagrams and general statements from bifurcation theory, to infer knowledge of the underlying global dynamics. The diagrams are generated with the method of numerical continuation, in this case using the software package AUTO [31] incorporated into the Matlab Dynamical Systems Toolbox [32]. The line types and symbols adopted here to define whether solutions are equilibria or limit cycles, stable or unstable, and to denote bifurcation points are listed in Table 1.

Note that a one-parameter bifurcation diagram for an n^{th} -order system occupies $(n + 1)$ -dimensional space; bifurcation diagrams are shown as 2D projections of this space, i.e. one state versus the chosen continuation parameter. Selected projections are shown, aimed at revealing the main features of the behaviour.

3.1 Open-loop characteristics

The open-loop system is 8^{th} -order, with state vector $[\alpha \ \beta \ V \ p \ q \ r \ \theta \ \phi]$. This omits the ψ and ground-position states of the system described in equation (4) since these play a negligible role in the flight dynamics behaviour of the aircraft. Figure 4 shows the α and p projections of the open-loop system bifurcation diagram for the GTM. The starting solution was a trim point at a prescribed altitude and angle of attack: 800 ft (243m) and $\alpha = 3^\circ$; the associated forward speed is $V = 47.3\text{m/s}$. The corresponding parameter values are: throttle 22.1%, elevator deflection $\delta_e = 2.58^\circ$ and aileron and rudder close to zero (-0.004° and 0.009° respectively). In addition to the small thrust asymmetry in the model, the aerodynamics is not symmetric about the x - z plane for zero aileron and rudder. The asymmetry is, however, very small at low angles of attack. Aileron, rudder and throttle remain fixed at these values, whilst δ_e is the continuation parameter.

The behaviour shown in Fig. 4 is described in detail in Ref. [12]. The salient types of behaviour are labelled A–G and summarised in Table 2.

Table 2: Summary of characteristics of GTM open-loop behaviour in Fig. 4 (from [12]).

Symbol	Type of Dynamics	α range
A	Stable trimmed symmetric flight	-2° to 8°
B	Low frequency oscillations	2.2° to 21°
C	Steady steep spiral	10.5° to 20.9°
D	Inverted spiral	-5° to -2°
E	Steady steep spin	30.5° to 38.8°
F	Period-one oscillatory steep spin	32.7° to 38.5°
G	Period-three oscillatory steep spin	30.8° to 40°

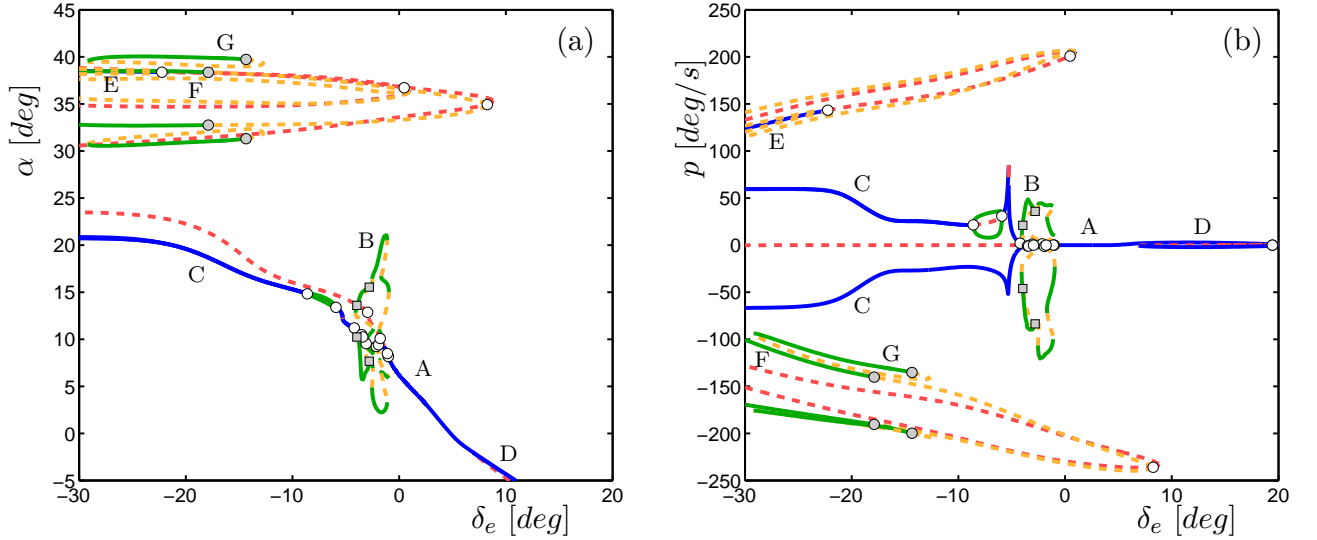


Figure 4: Open-loop bifurcation diagram in angle of attack (a) and roll rate (b), from [12].

Of specific interest in terms of upset are the steady steep spirals C, the steady spin E and the two oscillatory spins F and G. The steep spirals of regime C exist for both positive and negative p and form descending spirals to the right and left respectively. Angular rates are reasonably large with p exceeding $60^\circ/s$ and along with this, $\phi \approx \pm 60^\circ$ and flight path angle, γ , reaches -70° . For these reasons, regime C can be classified as an upset condition, within the requirements designated by both the URTA [29] and Lambregts et al [30]. The steady spin of regime E was found to exist only for positive p and is characterised by large angular rates and $\gamma \approx -89^\circ$, indicating that, in this regime, the GTM would be falling near to vertical. However, it was found that, although this dynamic regime is also a serious upset condition, it is a weak attractor and time history simulations were unable to access the branch without being exactly initialised on it; they were attracted to the steep spiral of regime C.

The two oscillatory spins, however, represent much stronger attractors in the open-loop GTM. These also exhibit large angular rates and large negative γ but were found to be accessible for the GTM by the use of large rudder inputs at high pitch up elevator [12]. Regime F is a period-one periodic orbit with a time period of $\approx 1s$ while regime G is a period-three periodic orbit with a time period of $\approx 3s$. The small time period of these oscillations, along with the angular rates and γ , infer that these periodic orbits can be classed as upset by the criteria described and, in fact, represent the most severe form of upset exhibited by the open-loop GTM.

3.2 Closed-loop characteristics

3.2.1 α_{cmd} bifurcation diagrams – controller \mathcal{C}_1

The controller \mathcal{C}_1 was designed for a single trim condition at $\alpha = 4.28^\circ$ and $V = 41.2m/s$ whilst for \mathcal{C}_2 a series of such $\gamma = 0$ trims were used. This condition yields an implicit dependency between α_{cmd} and V_{cmd} . This dependency is replicated in the generation of bifurcation diagrams for the closed-loop system: the same trim function as that adopted in the controller design was used to define a schedule of V_{cmd} inputs versus continuation parameter α_{cmd} ; this schedule was then implemented during the numerical continuation runs such that V_{cmd} and, hence, throttle setting, also change as α_{cmd} varies. This means that the branch of trim solutions on the bifurcation diagrams corresponds directly with the conditions previously used to assess the controllers and ensures symmetric trim solutions with $\gamma = 0^\circ$.

In this analysis, a reduced-order model of the GTM was used to characterize the stability of the system in order to relate results to that used in the control law design process. This incorporated the fast-varying states $[\alpha \ \beta \ V \ p \ q \ r]$; the slow varying modes (spiral and phugoid) are ignored in this analysis because their instability can be easily controlled by either the pilot via reference commands, or an autopilot. The bifurcation analysis,

on the other hand, incorporates all 8 flight dynamics states.

Figure 5 shows the α , p , q , ϕ , θ and δ_r projections of the closed-loop bifurcation diagram with α_{cmd} as continuation parameter. The chosen range for α_{cmd} is 0° - 30° , as this encompasses the range considered during the controller design and evaluation. The p and β projections (not shown) yield equilibrium solutions that are zero as this is the commanded value, i.e. the p_{cmd} and β_{cmd} systems are able to meet their objective in terms of steady state behaviour throughout the incidence range shown. For the majority of the chosen α_{cmd} range, α also matches its target equilibria values; however, this becomes unachievable for $\alpha_{cmd} \geq 23^\circ$ on the non-symmetric branch, due to position saturation of the elevator. Note: in this implementation, control surface position saturation is modelled by the use of smoothly blended piecewise functions.

Table 3: Summary of characteristics of GTM closed-loop behaviour (controller \mathcal{C}_1) in Fig. 5.

Symbol	Type of dynamics	Approx. α_{cmd} range
A	Symmetric equilibria: unstable spiral but fast modes (6^{th} -order system) stable	0° to 12° and 12.7° to 21°
B	Low-amplitude limit cycle in stall region	12° to 12.7°
C1	Stable equilibria: helical turn ($+\phi$)	0° to 12° and 12.7° to 20.3°
C2	Stable equilibria: helical turn ($-\phi$)	0° to 12° and 12.7° to 21°
D1	Low-amplitude limit cycle in stall region on C1	12° to 12.7°
D2	Low-amplitude limit cycle in stall region on C2	12° to 12.7°
E	Large amplitude unstable limit cycle	21° to 22.5° (aileron saturation)
F1	Large amplitude stable limit cycle from C1	20.3° to 22° (elevator saturation)
F2	Large amplitude stable limit cycle from C2	21° to 22° (elevator saturation)

We observe from Fig. 5 that the controller ensures that the trimmed equilibria in p , q and ϕ are indeed symmetric in nature, whereas the open-loop steady states are noticeably asymmetric (Fig. 4) except in region A. Evidence of the asymmetry is, however, reflected in the rudder (δ_r) plot, as well as in the aileron states (not shown). The types of behaviour on the various solution branches in Fig. 5 are summarised in Table 3. The closed-loop symmetric trim solution branch (marked ‘A’ in Fig. 5) is unstable, and this is due to the slow spiral mode (the 6^{th} -order system does not reflect this instability as it omits the slow spiral and phugoid dynamics). However, the time-to-double-amplitude for this mode is large: handling qualities are considered to be acceptable (‘level 1’ in conventional handling qualities terminology [33] which corresponds to ‘satisfactory’ in [34]) for α_{cmd} up to 19.3° and hence so is the control law in this respect. Solutions meeting this time-to-double-amplitude level 1 handling qualities criterion are indicated 6-state stable using the light blue line type (shown in table 1) in the closed-loop bifurcation diagrams.

In the stall angle-of-attack region, however, there is a further instability in the form of a complex pair of eigenvalues crossing into the right-half plane; the resulting bifurcation at $\alpha_{cmd} = 12^\circ$ gives rise to periodic orbits (marked ‘B’) which grow in amplitude and then reduce again, disappearing in another bifurcation at $\alpha = 12.7^\circ$. The loss of stability of what appears to be the short period mode over this small region does represent a deficiency in the fixed-gain controller, although the consequences would not be considered dangerous in the context of loss-of-control or upset; in fact, the amplitude is sufficiently small that in Fig. 5 it is only really visible in the q projection. A further Hopf bifurcation point arises at $\alpha = 21^\circ$. An unstable limit cycle is born at this point (‘E’); the aileron deflections saturate at $\alpha \approx 22.5^\circ$ and the orbits remain unstable until at least $\alpha = 30^\circ$.

Before discussing the other solution branches in Fig. 5, we consider the ‘root locus’ associated with the symmetric branch: i.e. the locus of eigenvalues as the continuation parameter, α_{cmd} , varies (rather than in the conventional sense where a controller gain varies). Figure 6 shows, in panel (a), this root locus for the 6^{th} -order system with the controller \mathcal{C}_1 (left-hand plot) and, in panel (b), the corresponding variation of the real parts of these roots with angle of attack (right-hand plot). Since the controller ensures an effectively symmetric flight condition through the α_{cmd} range, the eigenvalues of the linearized system can be separated into those representing longitudinal modes and those representing lateral/directional modes. Loci in red are longitudinal and those in blue are lateral-directional. These plots confirm that the limit cycle in the $\alpha = 12^\circ$ region, corresponding to a complex pair of roots crossing into the right-half plane, is due to a loss in longitudinal

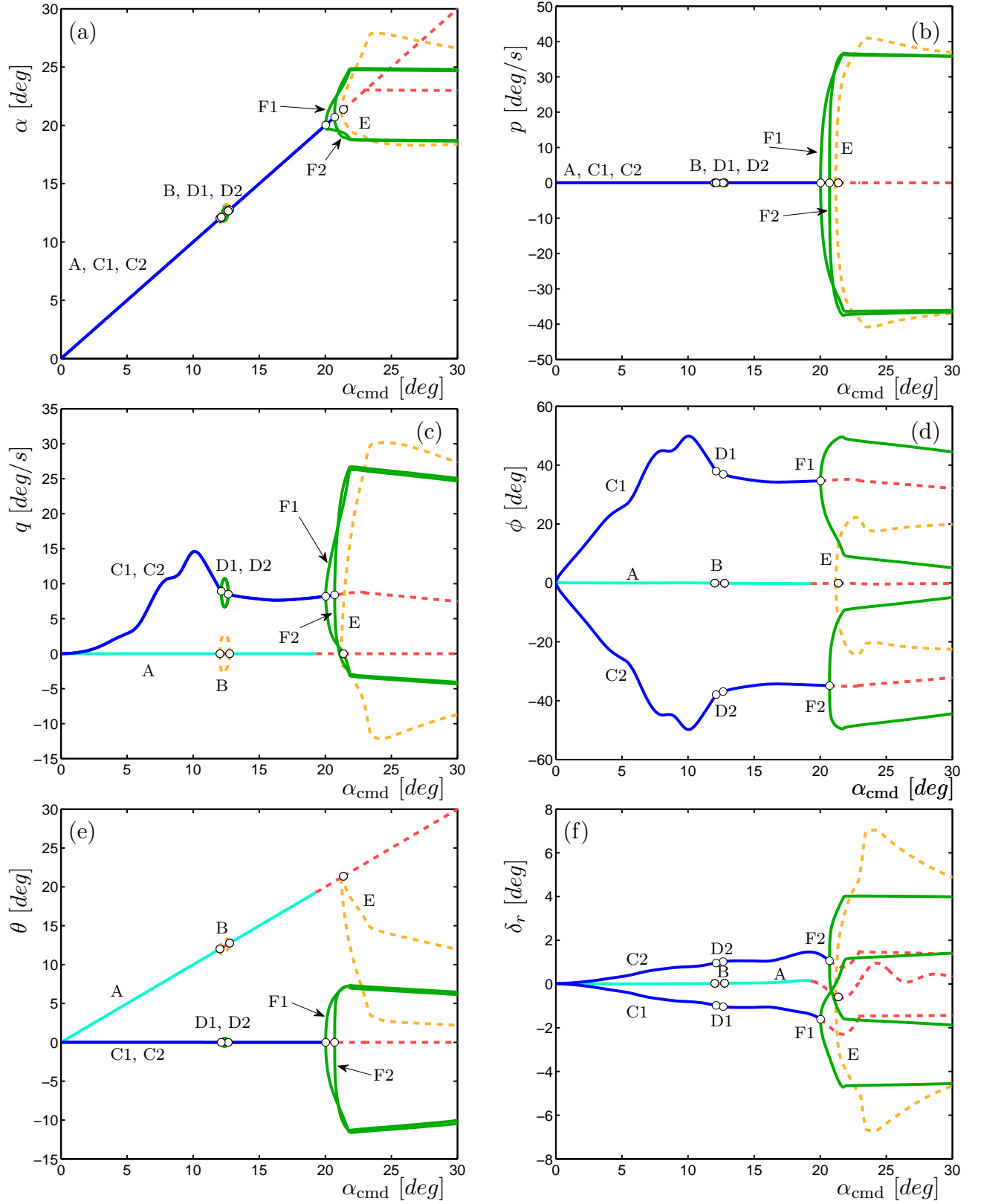


Figure 5: Closed-loop bifurcation diagram, for controller \mathcal{C}_1 : panels (a)-(f) show α , p , q , ϕ , θ and δ_r projections, respectively.

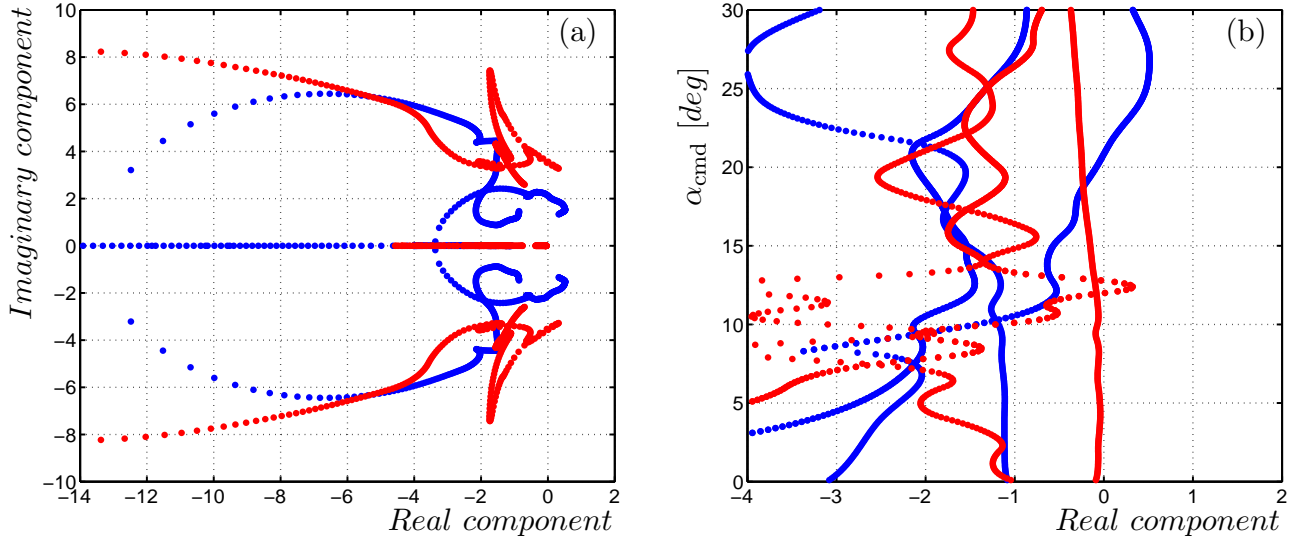


Figure 6: Closed-loop root locus for the 6th-order system (a), and corresponding variation of real parts with angle of attack (b), for symmetric solution branch and controller C_1 . Red loci are longitudinal roots and blue lateral-directional.

stability. We also see that a lateral-directional root enters the right-half plane at $\alpha = 21^\circ$, causing the Hopf bifurcation in Fig. 5.

In addition to the symmetric solution branch discussed above, we note in Fig. 5 that there are two branches of stable equilibria arising at zero angle of attack (denoted ‘C1’ and ‘C2’). These are close to anti-symmetric in the lateral-directional sense (i.e. the value of β , p , r or ϕ at a particular α_{cmd} on C1 is virtually equal in magnitude and is of opposite sign to that on branch C2, whilst the longitudinal variables are equal in value and sign on C1 and C2). Close inspection of these solutions shows that they represent helical trajectories – descending turns – with pitch angle $\theta = 0^\circ$. This is due to the kinematics of an aircraft constrained in a turn with zero roll rate, due to the $p_{\text{cmd}} = 0$ function in the controller. In particular, consideration of the $\dot{\phi}$ and $\dot{\theta}$ kinematic equations under equilibrium conditions with $p = 0$ reveals that $r \tan \theta$ must be zero. For the symmetric solution branch, denoted A in Fig. 5, yaw rate is zero so that $r \tan \theta$ will be zero whatever the value of θ ; however, for the turning solution where $r \neq 0$, pitch angle θ must be zero for the kinematic constraint to be met. By definition $\gamma = \theta - \alpha$ so that the helical turn solutions in the bifurcation diagram, where $\alpha_{\text{cmd}} \geq 0$, require γ to be negative – denoting descending flight.

It is worth comparing the ‘off-nominal’ behaviour of the closed-loop aircraft helical turn solutions with those of the open-loop steep spirals indicated as regions C in Fig. 4. The flight path angle for the closed-loop descending turns is substantially lower than that of the open-loop steep spiral, where γ reaches -70° . Also, the groundtrack radius, calculated by simulation of the full nonlinear 12th-order system, is far tighter for the open-loop spiral; in fact, an order of magnitude smaller than the helical turn radii. Comparing the behaviour of the helical turns with that considered upset the only condition exceeded is that $\phi \geq \pm 45^\circ$ and even then this is just for the portion of the branches between $7^\circ < \alpha_{\text{cmd}} < 11^\circ$. Thus the stable portions of the descending turn solution branches do not reflect upset conditions for the majority of the α_{cmd} range, unlike the open-loop steep spiral, showing improved upset behaviour with the addition of controller C_1 .

As with the symmetric branch, the turning solutions also lose stability in the $\alpha = 12^\circ$ - 12.7° range associated with wing stall for this small-scale airliner configuration. Again, the amplitudes of the resulting limit cycles (D1 and D2) are small and only really visible in the projections of q in Fig. 5(c). Furthermore, there are additional Hopf bifurcation points on these branches in the region of 20° - 21° incidence – again mirroring the loss of stability at a similar incidence on the symmetric branch. These are supercritical Hopf points, where the periodic orbits (F1 and F2) that grow from them are stable; they increase in amplitude as α_{cmd} increases until the elevator and ailerons saturate during parts of the orbits (as from $\alpha_{\text{cmd}} \approx 22^\circ$) and maintain stability until at least $\alpha_{\text{cmd}} = 30^\circ$. This mirrors periodic orbit E from the symmetric branch. The very slight asymmetry

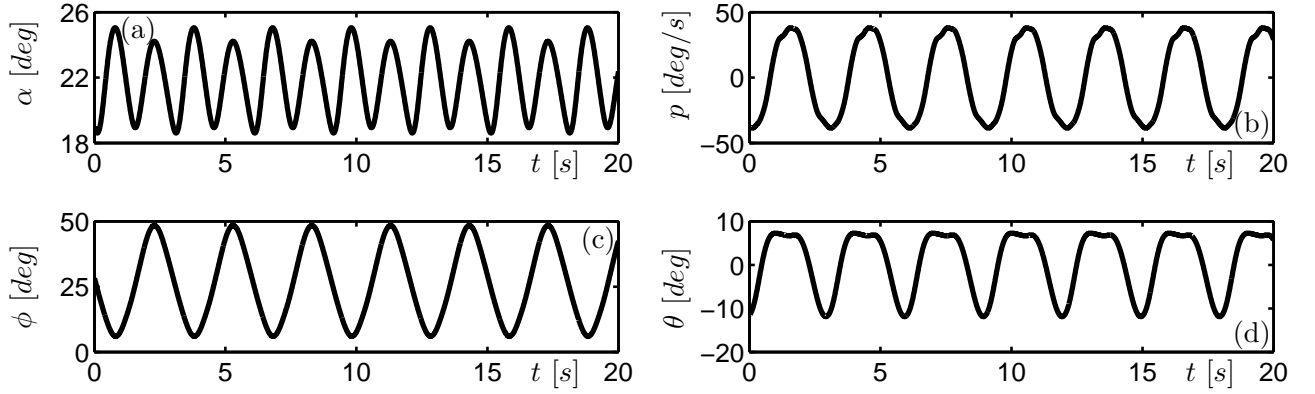


Figure 7: Closed-loop time history with α_{cmd} fixed at 23° on the oscillatory turn for controller \mathcal{C}_1 . Panels (a)-(d) show α , p , ϕ and θ responses, respectively.

present in the system on these anti-symmetric branches is not easy to observe in Fig. 5, although the difference in α_{cmd} values at which the F1 and F2 limit cycles occur on each of the two branches is visible.

The time history of periodic orbit F1 with α_{cmd} fixed at 23° shown in Fig. 7 implies that this periodic orbit is a much more dangerous flight condition than those on the stable parts of the C1 helical turn branch. Although altitude is lost more slowly during this oscillating turn than in the open-loop steep spiral and steep spin solutions, the rapid large magnitude roll excursions could induce excessive loads on the aircraft. Hence, even though the flight parameters lie within that often considered upset by the URTA, periodic orbits F1 and F2 can be considered as potential upset solutions due to the large rate of change of attitude. However, the bifurcation diagrams indicate that recovery away from these attractors can be simply attained by reducing α_{cmd} to below the value at which the Hopf bifurcations occur; this will return the aircraft to a stable descending turning solution.

3.2.2 α_{cmd} bifurcation diagrams – controller \mathcal{C}_2

As described in Section 2.3, controller \mathcal{C}_2 is gain scheduled based on three trim points at angles of attack corresponding to cruise, stall and post-stall flight conditions (4.28° , 13° and 22° , respectively). Given the bifurcation diagrams shown thus far, these design points are seen to be well suited to accommodate the nonlinear nature of the GTM dynamics and so we would expect a well-designed gain scheduled controller to stabilize the solutions through the limit cycle regions described above for the fixed-gain controller (i.e., referring to Fig. 5/Table 3, around points B, D1 and D2 in the 12° - 13° angle of attack region and points E, F1 and F2 above 20° angle of attack).

Figure 8 shows the α , p , q and ϕ projections of the bifurcation diagram for controller \mathcal{C}_2 ; it was generated as that for controller \mathcal{C}_1 shown in Fig. 5, i.e. again using α_{cmd} as the continuation parameter and with the same V_{cmd} schedule to maintain $\gamma = 0$ on the symmetric branch.

By evaluating the time-to-double-amplitude, the unstable spiral mode on the symmetric branch now satisfies, for \mathcal{C}_2 , the level 1 handling quality criterion up to a slightly higher angle of attack ($\alpha_{\text{cmd}} = 21.5^\circ$) than that for the fixed-gain controller \mathcal{C}_1 . More importantly, it is evident from the bifurcation diagram in Fig. 8 that the gain-scheduled controller \mathcal{C}_2 stabilises all the periodic orbits that were exhibited on both the symmetric and the helical turn solution branches in the case of controller \mathcal{C}_1 . This implies that \mathcal{C}_2 stabilises the aircraft throughout the useable α_{cmd} range.

3.3 Application of the gain parameter to all controller gains

The principal interest in using bifurcation methods to assess the impact of control laws is to investigate off-nominal conditions and, in particular, the influence of attractors associated with unwanted behaviour – including upset. The open-loop GTM is prone to entering the steep spiral region (C in Fig. 4), which can be considered a form of upset behaviour; it can also enter the oscillatory spin regions (F and G in Fig. 4) which are, of

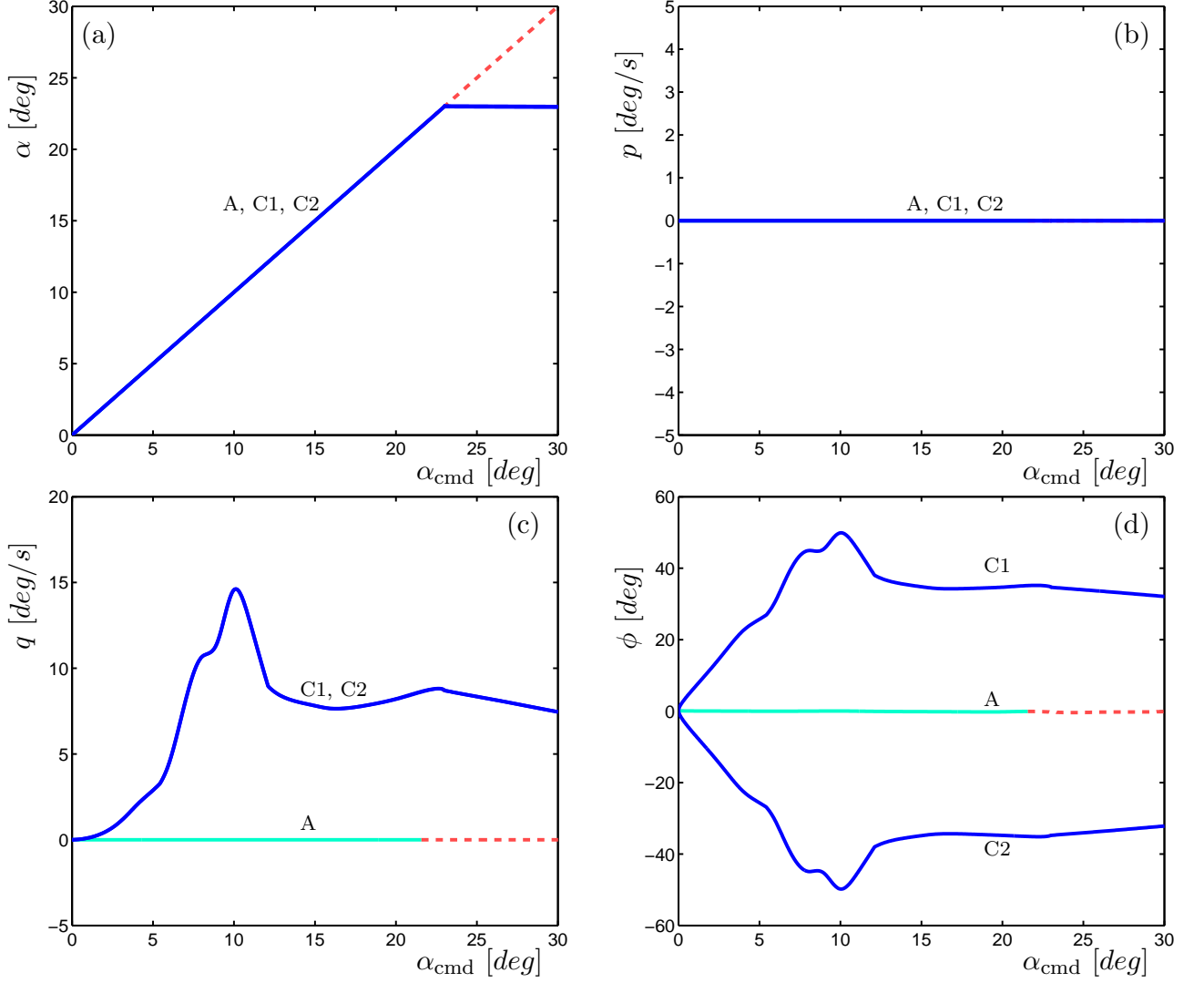


Figure 8: Closed-loop bifurcation diagram, controller C_2 : panels (a)-(d) show α , p , q and ϕ projections, respectively.

course, particularly dangerous (although recoverable). A flight controller has the potential of modifying such a behaviour but might not be able to fully eradicate it: the solution branches representing undesirable behaviour may move in state-parameter space but could potentially still play a role in inducing upset conditions when, for example, the aircraft is subject to a large disturbance. In order to investigate these effects, we carry out numerical continuation with a ‘gain parameter’, GP, as the continuation parameter to represent the transition from open- to closed-loop. This so-called ‘homotopy’ parameter is simply a factor applied to one or more of the controller gains, such that when GP=0 the gains are zero (open loop) and when GP=1 the relevant gains are at their design values for the controller under consideration. It can also be increased beyond 1 to explore the stability margins of the controller. This analysis enables determining a range of controller gains for which the controller is effective.

Figure 9 shows this open-to-closed-loop transition when continuation parameter GP is applied to *all* the gains, i.e. those on the command paths and those on the stability augmentation paths. The continuation was initiated at the point GP=1 and then the controller gains were varied away from the design point in both negative and positive directions to investigate the performance of controllers that are less and more aggressive relative to the baseline controller respectively. To carry out this analysis, consideration must be given to the

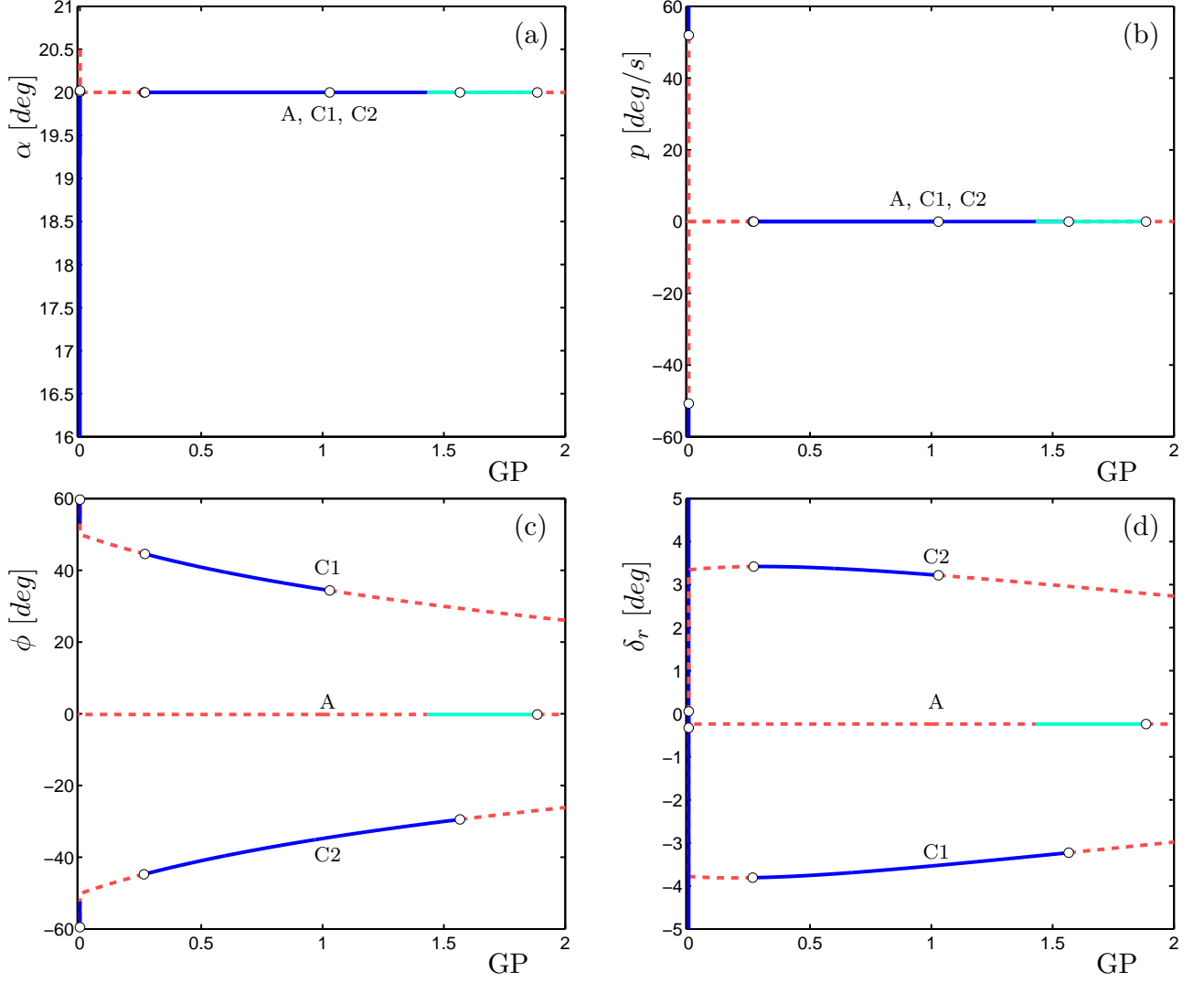


Figure 9: Closed-loop bifurcation diagram, for controller C_1 : panels (a)-(d) show α , p , ϕ and δ_r projections, respectively. Continuation is with respect to the gain parameter, GP.

constant values used for the controller commands since the GP=0 and GP=1 points may be very different flight conditions, especially at GP=0 which is equivalent to open-loop flight. In this case, controller commands corresponding to symmetric trim at $\alpha_{\text{cmd}} = 20^\circ$ were chosen, because this was close to the point of lateral-directional instability that manifests itself in periodic orbits E, F1 and F2 in Fig. 5. As the gain parameter is varied, the controller commands remained fixed at their $\gamma = 0$ trim settings for $\alpha = 20^\circ$, namely $\alpha_{\text{cmd}} = 20^\circ$, $V_{\text{cmd}} = 49 \text{ m/s}$ and $p_{\text{cmd}} = \beta_{\text{cmd}} = 0$. This gives rise to an ‘instantaneous’ demand on the controlled variables as soon as GP increases above zero, which is particularly evident in p and β as their commanded values are far from those in open-loop.

It is evident from Fig. 9 that, when the controller is operative (GP>0), it attempts to drive the states to the pilot commands, even when the gain is very small. This results in a very dramatic change in the equilibrium solutions as the gain increases slightly from zero. The jump in α is only present in the two equilibrium branches where $\phi \neq 0$ and not for the symmetric branch. This is the case because the controller is trimmed for the symmetric branch at $\alpha = 20^\circ$: the elevator deflection for this condition is $\delta_e = -11.95^\circ$ but whilst for open-loop this elevator deflection ensures that $\alpha = 20^\circ$, for the steep spiral – the non-symmetric branches in Fig. 9 – an elevator deflection of $\delta_e = -11.95^\circ$ gives $\alpha \approx 16^\circ$. The jump arises from the α_{cmd} path of the control law

and decreases δ_e until $\alpha = 20^\circ$ is achieved. Note that, while the controller is able to significantly alter the equilibria for even a very small gain, any transient dynamics here are likely to be rather slow. As the controller is ‘turned on’, the state variables move to the commanded values, even if the control gains are tiny; the other uncommanded states vary as GP varies and reach the full closed-loop values when GP=1. However, at small gains (where $GP \leq 0.25$), stability is lost on all three branches at Hopf bifurcations.

This form of continuation run reveals the potential for the continuation and bifurcation analysis technique to provide insight into the impact of controller changes, both near and away from nominal design conditions. In the case considered here, the controller gains must be greater than a quarter of the nominal value in order to achieve stability. Figure 9 also indicates that to achieve level 1 spiral mode handling qualities on the symmetric branch for C_1 at $\alpha = 20^\circ$, the parameter GP needs to be in excess of about 1.45 (cf. Fig. 5 where the spiral mode rate of divergence no longer meets level 1 handling quality levels once α_{cmd} exceeds 19.3°).

Other smoothly-varying controller characteristics could also be evaluated in the same way, allowing insight into closed-loop behaviour in regions away from the baseline controller; such characteristics may not be identified when only conventional linear methods are deployed. The gain parameter bifurcation diagram for the controller C_2 in Fig. 10 shows similar behaviour. Due to the gain-scheduling, the nominal value of the gains of this controller are larger than those of C_1 at $\alpha_{cmd} = 20^\circ$ and, hence, the system loses stability on the descending turn branches only once GP is reduced below about 0.15. Also, for the symmetric branch, controller C_2 maintains level 1 handling qualities for GP values down to approximately 0.5 which represents superior performance over C_1 .

From Figs. 9 and 10 it is clear that, as soon as the controller is activated, the open-loop steep spiral solution is ‘converted’ into the helical turn solution. In addition to all the commanded states switching to their command values, $\theta \rightarrow 0$ as $p \rightarrow 0$ due to the kinematic effect described above. This descending turn behaviour is acceptable and certainly preferable from a safety perspective to the dangerous open-loop steep spiral. Figure 11 compares the open-loop spiral and the closed-loop descending turn solutions by depicting their trajectories. This confirms that, while the open-loop spiral is a rapid rotation with small radius, the closed-loop response is far slower (a full turn takes approximately five times longer than in the spiral) and with a substantially larger radius.

Figure 5 revealed that the helical turn equilibria lose stability at $\alpha \approx 21^\circ - 22^\circ$ for controller C_1 . The choice of $\alpha_{cmd} = 20^\circ$ for generating the gain parameter bifurcation diagram of Fig. 9 means that the system steady states are close to becoming unstable. Indeed, we observe that, if GP is increased just beyond a value of 1, the C_1 (positive ϕ) turning solution in Fig. 9 loses stability at a Hopf bifurcation. This indicates that, at this point, controller C_1 has limited stability margin. The branch C_2 (negative ϕ) does not lose stability until $GP \geq 1.55$, which shows that the descending turn with negative ϕ is a more robust solution than that for positive ϕ . This difference is likely due to the asymmetry of the physical GTM aircraft mentioned in section 3.1 rather than the controller. The loss of stability of C_1 so close to the nominal controller gains would not be expected – although it is clear that the controller C_1 is operating far away from the design point of $\alpha = 4.28^\circ$. This potential lack of robustness is not seen in the bifurcation diagrams for controller C_2 in Fig. 10, which has a gain-scheduling design point at $\alpha = 22^\circ$. The dependence of such features on parameter variations is clearly portrayed via the bifurcation diagrams and these suggest that the gain-scheduling of controller C_2 is significantly more robust than C_1 at high angles of attack.

The structure of the control law (integral control over integral error states) is such that the steady state solutions adopt the commanded values even for extremely small gain parameter. This is ‘just beyond’ open-loop and is due to the integral terms on the command path which will increase in magnitude until the command values or the control surface limits are reached. Provided that there is sufficient control power, the integrator will always reach the commanded values in the steady state. However, in practice the transient response would be slow if the gains were small because the integrators would take considerable time to respond to the commands (even if the equilibrium was stable). In the example for C_1 shown in Fig. 9 the helical turn equilibria are all unstable for $GP \leq 0.25$. The periodic solutions which would arise from the Hopf bifurcations have not been considered here, as the primary interest for the design of controller gains is the point where the controllers lose stability rather than the behaviour past this point.

Figure 12 shows the responses in α for a number of time histories, each for controller C_1 , with different values of GP corresponding to Fig. 9 – ranging from 0.01 to 1. In each case, the simulation starts with GP=0 (open loop) and the GP value ramps up linearly to the new non-zero value over the time interval from 50 to 51 seconds. The responses for GP=0.01 and GP=0.1 exhibit the expected unstable behaviour for controller C_1 at low gain parameter. At GP=0.1 the solution is periodic but for GP=0.01, the solution is more complex

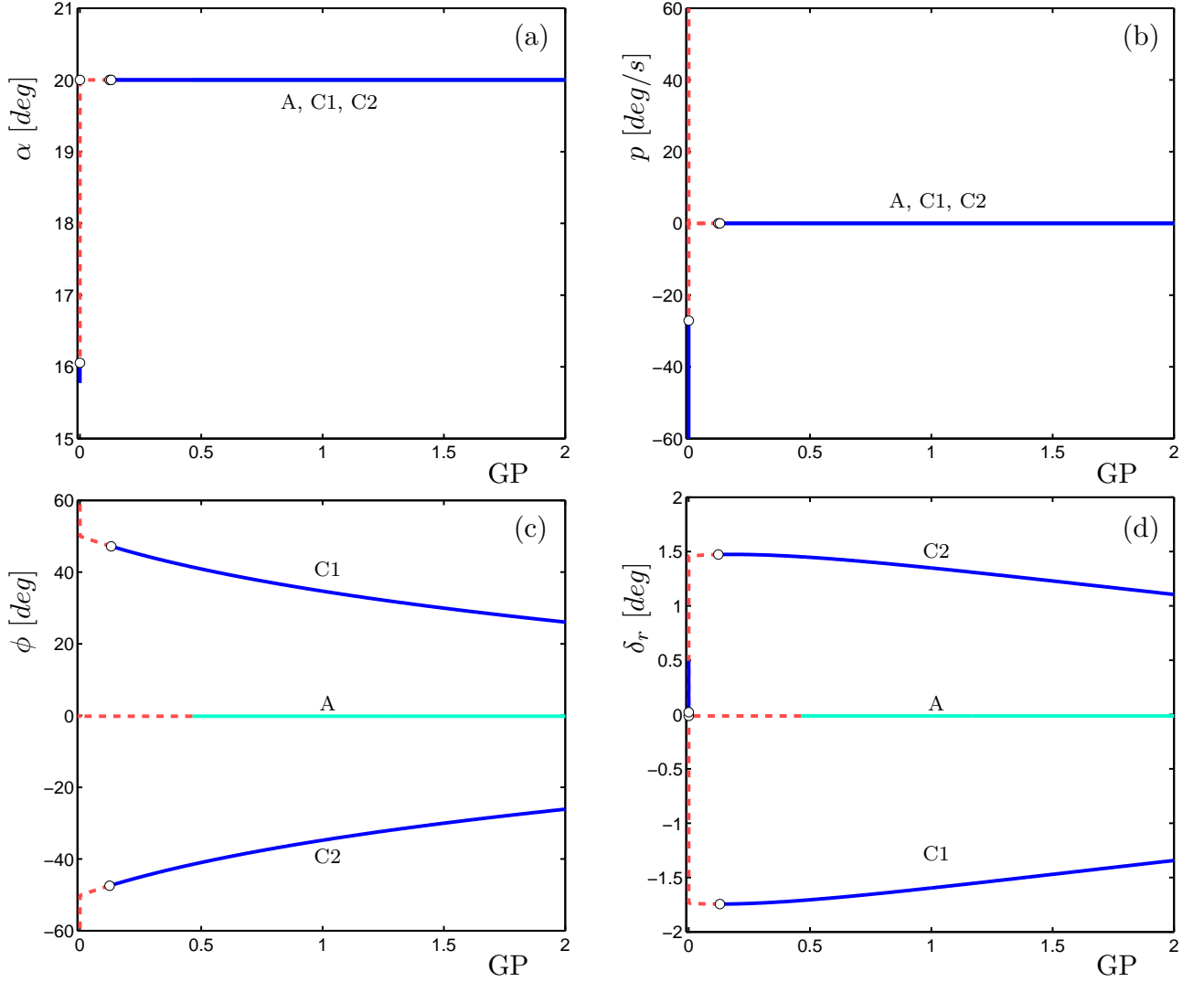


Figure 10: Closed-loop bifurcation diagram, for controller C_2 : panels (a)-(d) show α , p , ϕ and δ_r projections, respectively. Continuation is with respect to the gain parameter, GP.

and the amplitude varies significantly. For values of GP higher than 0.25, we expect a stable response. This is evident for GP=0.3, 0.5 and 0.8 but when GP=1 a periodic orbit is induced. This is, at first glance, unexpected as the equilibria are stable for GP=1, and it implies that controller C_1 is particularly bad at dealing with this upset condition. As noted, the bifurcation diagrams in Fig. 5 show that the $\alpha_{\text{cmd}} = 20^\circ$ solution is very near a Hopf bifurcation, which explains why in the presence of a disturbance the response appears to be approaching a limit cycle rather than an equilibrium solution. This suggests that the Hopf bifurcation in the gain parameter projection is subcritical. For the gain-scheduled controller C_2 , Fig. 8 indicates that there are no bifurcations and indeed Fig. 10 shows that there are no instabilities present at GP=1.

In terms of flight upset, of greater concern is the impact of both the controllers on the oscillatory spin solutions (regimes F and G in Fig. 5) that are present in the open-loop system. As described in [12], these spins are very dangerous upset conditions with oscillations around an angle of attack of $\alpha \approx 35^\circ$. Here, the aerodynamics are very nonlinear and control effectiveness is reduced due to airflow separation. Interestingly, the bifurcation diagrams of the closed-loop system for both C_1 and C_2 imply that the GTM does possess sufficient control authority to allow the command path to eliminate the oscillatory spins. Oscillatory solutions at high α do exist for the fixed-gain controller C_1 , although the angles of attack in this ‘oscillatory turn’ are in the vicinity

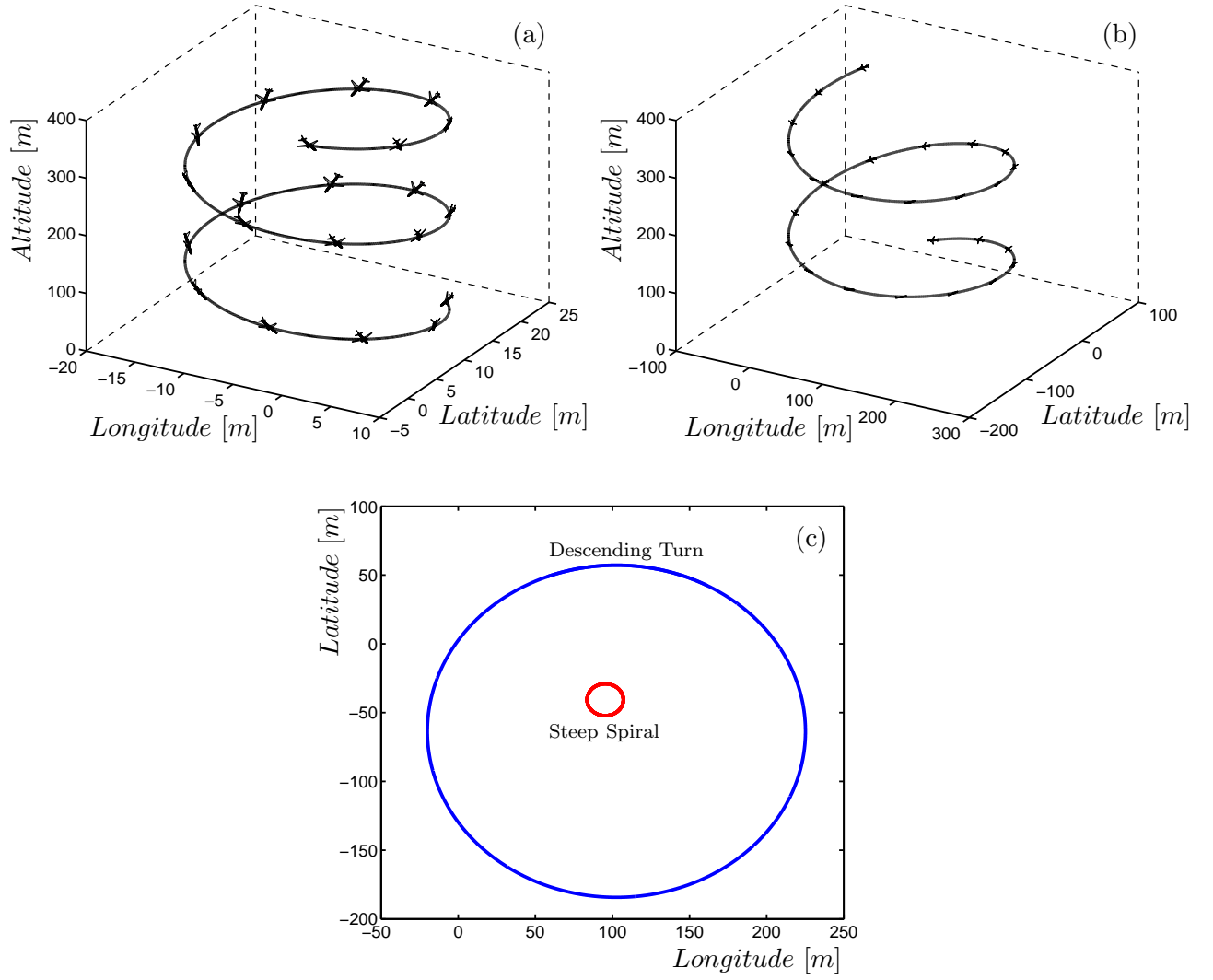


Figure 11: Open-loop steep spiral trajectory (a), closed-loop descending turn trajectory (b) and comparison of ground track for the two cases (c).

of $\alpha = 20^\circ$ rather than 35° and behaviour is, therefore, likely to be dominated by aerodynamic phenomena different from those of the open-loop oscillatory spins.

In considering the GTM with controller \mathcal{C}_1 we, therefore, see that whilst the open-loop oscillatory spins at $\alpha \approx 35^\circ$ may be absent, there is now the possibility of oscillatory solutions arising at a far lower angle of attack than in the open-loop case – down to $\alpha \approx 20^\circ$ (arising from both the symmetric and the asymmetric, helical turn solution branches). Any situation that causes the incidence to rise to this level is likely to result in highly undesirable upset-type dynamics. For the open-loop aircraft it is reasonably challenging (but possible) to transition from the steep spiral equilibria to the oscillatory spin; in the case with fixed-gain controller \mathcal{C}_1 , a large pitch perturbation could push the aircraft into an oscillatory upset scenario relatively easily. However, the bifurcation diagrams indicate that decreasing α_{cmd} will recover the vehicle to well-behaved equilibrium flight – a consequence of having a controller that tracks α_{cmd} by generating inputs that depend on integral error states.

3.4 Application of the gain parameter to stability augmentation gains

In order to further investigate the impact of the control law on the spin regime and to assess the attributes of the bifurcation method, the gain parameter method described earlier was applied to the stability augmentation

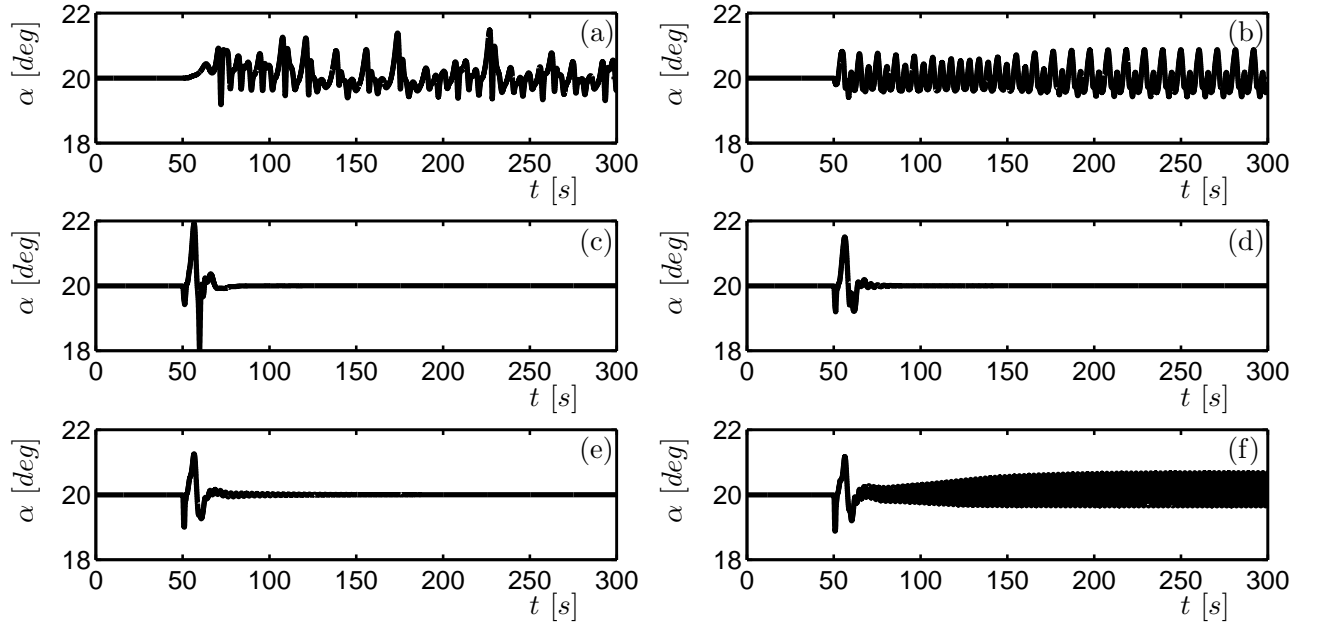


Figure 12: Angle of attack time histories, controller \mathcal{C}_1 , for GP ramped from zero to a value of 0.01, 0.1, 0.3, 0.5, 0.8 and 1 in panels (a)-(f), respectively. In each run, GP is zero up to time=50s, then ramped linearly to the indicated value over the interval of 50 to 51s, after which it is fixed.

path of the controller only. The command path integrator gains and the auto-throttle were disabled. The stability augmentation path uses purely proportional gains and consists of a total of nine separate paths. Both longitudinal and lateral-directional stability augmentation gains were used. We refer to this combination of gains as the ‘proportional gains’ and the gain parameter applied to them as GP_{SA} .

Figure 13 shows the α , p , ϕ and δ_r projections of a bifurcation diagram for controller \mathcal{C}_1 in which GP_{SA} , applied to all proportional gains, is varied from 0 up to 1 (recalling that $\text{GP}_{\text{SA}}=1$ corresponds to the \mathcal{C}_1 design gain values). Where $\text{GP}_{\text{SA}}=0$, the solution branches are equivalent to that of the open-loop system bifurcation diagram, Fig. 4, at $\delta_e = -24^\circ$. The value of $\delta_e = -24^\circ$ was chosen because, at this elevator deflection, both the open-loop steep spins, regimes F and G, are stable as are the steep spirals. The solution branch labels in Fig. 13 correspond to those for the open-loop system described in table 2 due to the deactivation of the command path. The stable equilibrium branches at $\alpha \approx 20^\circ$ are the steep spiral solutions and the high α periodic orbits are the oscillatory spins. It is evident that closing the loop for a set of suitable controller gains ($\text{GP}_{\text{SA}} \geq 0.35$) does eliminate the spin branches: they all undergo limit point bifurcations as GP is increased, ensuring that there are no local solutions in their vicinity for greater gain parameter values. Further analysis, using each individual gain as the continuation parameter, has revealed that the dominant gain in the elimination of the oscillatory spins is that of proportional yaw rate feedback to the rudder [35].

A similar study for the gain-scheduled controller \mathcal{C}_2 is shown in Fig. 14. It shows that \mathcal{C}_2 exhibits similar behaviour to \mathcal{C}_1 with respect to reducing the proportional gains. The main difference between the two controllers is that for \mathcal{C}_2 the limit point bifurcations, which signify where the spin solutions cease to exist, occur at an even lower gain parameter than for \mathcal{C}_1 . Hence, for \mathcal{C}_2 , spin solutions do not exist for a GP_{SA} greater than 0.12. For both controllers the negative roll rate spiral equilibrium solution branch remains stable throughout, whilst the positive roll rate equivalent includes an unstable region bounded by Hopf bifurcations. Although this region of oscillatory instability is very small for controller \mathcal{C}_2 , for \mathcal{C}_1 it was found to be much larger. For this fixed-gain controller, away from the Hopf bifurcation (at $\text{GP}_{\text{SA}}=0.4$), the resulting periodic orbit grows in amplitude very significantly. It is unstable until a limit point bifurcation is reached at $\text{GP}_{\text{SA}}=0.68$; the stable limit cycle that arises at the fold then exhibits multiple period doubling bifurcations as GP_{SA} decreases, indicating the presence of complex dynamics. Time histories (not shown) confirm that as GP_{SA} decreases, multi-frequency dynamics exists [35]. From an upset perspective, this is clearly a potentially dangerous operating regime.

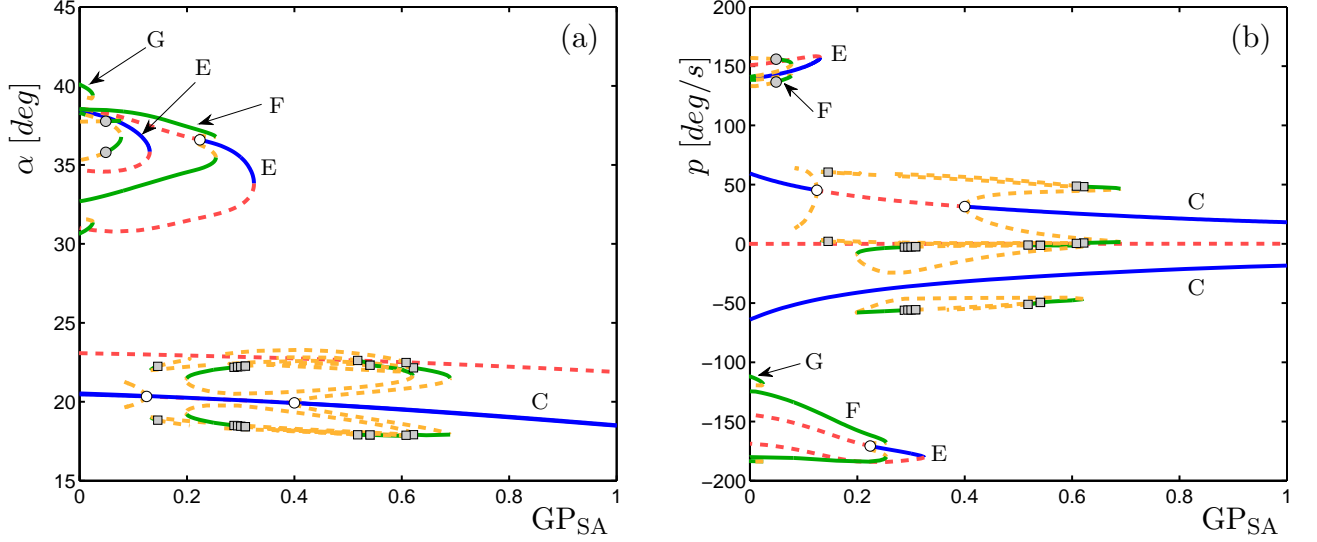


Figure 13: Closed-loop bifurcation diagram, $\alpha_{\text{cmd}} = -24^\circ$, controller \mathcal{C}_1 : panels (a)-(d) show α , p , ϕ and δ_r projections respectively. Continuation is with respect to the gain parameter, GP_{SA} , applied to all proportional gains; integral gains are zero, auto-throttle off.

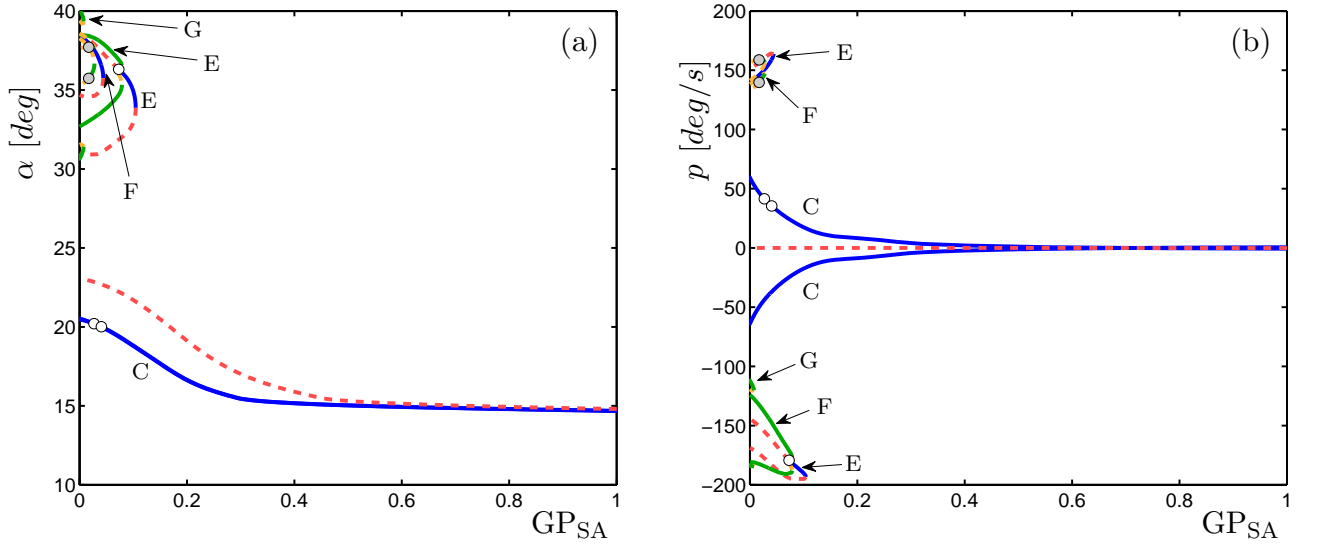


Figure 14: Closed-loop bifurcation diagram, $\alpha_{\text{cmd}} = -24^\circ$, controller \mathcal{C}_2 : panels (a) and (b) show the α and p projections respectively. Continuation is with respect to the gain parameter, GP_{SA} , applied to all proportional gains; integral gains are zero, auto-throttle off.

4 Concluding Remarks

The results shown here demonstrate that bifurcation analysis is an effective tool to evaluate how the flight control system alters the steady-state dynamics of aircraft throughout the flight envelope. Moreover, it allows one to determine the degree to which the behaviour improves (or degrades); and it provides an understanding of the dynamics that determine the responses observed in time history simulation. Since most controllers are not designed to cope with upsets, the reported analysis approach can be used to evaluate their effectiveness under operating conditions encountered during off-nominal, strongly nonlinear flying conditions. This analysis could

potentially be used to determine certain situations when it is beneficial to turn the controller off to recover from an upset.

Fixed-gain and gain-scheduled versions of a LQR-PI controller, designed to improve the behaviour of the Generic Transport Model, were studied. We focused on assessing the influence of the control laws not only for conventional symmetric trimmed flight but on off-nominal conditions too. The objective was to gain a better understanding of the susceptibility to upset for a closed-loop aircraft and to assess, where appropriate, recovery strategies. The approach taken in this paper is to exploit the nature of nonlinear dynamical systems – such as aircraft at high incidence – by employing bifurcation methods; in particular, we explored means of adapting these techniques to uncover the transition of the system attractors as the control loop is closed. In the results presented here, for both the fixed-gain and gain-scheduled controllers, the steep spiral exhibited by the open-loop GTM is transformed into a descending turn and the oscillatory spins are eliminated. An oscillatory turn, however, is induced for the fixed-gain controller, C_1 , and exists in the form of an unacceptable oscillatory response when the loop is closed. This behaviour is not observed for the gain-scheduled controller, C_2 , demonstrating the value of a nonlinear gain-scheduled controller for extending the region of stable/safe operation.

By conducting bifurcation analysis with respect to a homotopy parameter acting on one or more of the controller gains, we were able to gain insight into the effect of changes to the controller on the closed-loop dynamics. This provided a clear understanding of the influence of control law design on off-nominal conditions characterised by other, undesirable, steady state solutions being potentially present within the operating parameter space. This was illustrated in terms of the proximity to the closed loop limit cycles above 21° angle of attack for the fixed gain controller, and the changes in co-existing steep spiral and oscillatory spin branches caused by tuning proportional gains. Our analysis also shed light on which of the controller gains is dominant in eliminating the oscillatory spin. When applied to the gain scheduled controller, the approach revealed the expected superiority in stability relative to the fixed-gain controller, with the equilibria being bifurcation-free throughout the studied range – including near stall and above 21° angle of attack, so indicating greater robustness than the fixed gain controller.

Acknowledgements

The research of Stephen J. Gill is supported by a UK Engineering and Physical Sciences Research Council (EPSRC) studentship in collaboration with Airbus. We are grateful to colleagues in the NASA Langley Flight Dynamics Branch and Dynamics Systems and Control Branch for provision of the GTM model and advice on its use.

References

References

- [1] Chatrenet, D., “Air Transport Safety - Technology and Training,” *ETP 2010*, 2010, URL: <http://ec.europa.eu/invest-in-research/pdf/workshop/chatrenet%20.b3.pdf> [cited 10 June 2014].
- [2] Aviation Safety Boeing Commercial Airplanes, “Statistical Summary of Commercial Jet Airplane Accidents Worldwide Operations 1959 - 2012,” Tech. rep., Boeing Commercial Airplanes, 2013.
- [3] Balas, G. J., “Linear, Parameter-Varying Control and its Application to Aerospace Systems,” *23rd Congress of International Council of the Aeronautical Sciences*, 2002, ICAS 2002-5.4.1.
- [4] Khalil, H. K., *Nonlinear Systems: Pearson New International Edition 3rd Edition*, No. ISBN 978-1292039213, Pearson, Edinburgh Gate, Harlow, Essex, CM20 2JE, UK, 2002.
- [5] Slotine, J.-J. E. and Li, W., *Applied Nonlinear Control*, No. ISBN 978-0130408907, Prentice Hall, Englewood Cliffs, New Jersey 07632, USA, 1990.

- [6] Gregory, I. M., Cao, C., Xargay, E., Hovakimyan, N., and Zou, X., “L1 Adaptive Control Design for NASA AirSTAR Flight Test Vehicle,” *AIAA Guidance, Navigation, and Control Conference*, 2009, AIAA-2009-5738, DOI 10.2514/6.2009-5738.
- [7] Crespo, L. G., Matsutani, M., and Annaswamy, A., “Design of an Adaptive Controller for a Remotely Operated Air Vehicle,” *AIAA Journal of Guidance, Control and Dynamics*, Vol. 35, No. 2, 2012, pp. 406–422, DOI 10.2514/1.54779.
- [8] Jordan, T. L., Foster, J. V., Bailey, R. M., and Belcastro, C. M., “AirSTAR: A UAV Platform for Flight Dynamics and Control System Testing,” *AIAA Aerodynamic Measurement Technology and Ground Testing Conference, San Francisco, CA*, June 2006, AIAA-2006-3307, DOI 10.2514/6.2006-3307.
- [9] Foster, J., Cunningham, K., Fremaux, C., Shah, G., Stewart, E., Rivers, R., Wilborn, J., and Gato, W., “Dynamics Modeling and Simulation of Large Transport Airplanes in Upset Conditions,” *AIAA Conference on Guidance, Navigation, and Control*, San Francisco, CA, August 2005, AIAA-2005-5933, DOI 10.2514/6.2005-5933.
- [10] Abramov, N., Goman, M., Khrabrov, A., Kolesnikov, E., Fucke, L., Soemarwoto, B., and Smaili, H., “Pushing Ahead – SUPRA Airplane Model for Upset Recovery,” *AIAA Modeling and Simulation Technologies Conference*, Minneapolis, MN, August 2012, AIAA-2012-4631, DOI 10.2514/6.2012-4631.
- [11] Krauskopf, B., Osinga, H. M., and Galán-Vioque, J., *Numerical Continuation Methods for Dynamical Systems: Path following and boundary value problems*, No. ISBN 978-1-4020-6355-8 in Understanding Complex Systems Series, Springer-Verlag New York, Inc., 175 Fifth Avenue, New York, NY 10010, USA, 2007.
- [12] Gill, S. J., Lowenberg, M. H., Neild, S. A., Krauskopf, B., Puyou, G., and Coetzee, E., “Upset Dynamics of an Airliner Model: A Nonlinear Bifurcation Analysis,” *Journal of Aircraft*, Vol. 50, No. 6, 2013, pp. 1832–1842, DOI 10.2514/1.C032221.
- [13] Carroll, J. and Mehra, R., “Bifurcation Analysis of Nonlinear Aircraft Dynamics,” *J. Guidance, Control, and Dynamics*, Vol. 5, No. 5, 1982, pp. 529–536, DOI 10.2514/3.56198.
- [14] Guicheteau, P., “Bifurcation Theory Applied to the Study of Control Losses on Combat Aircraft,” *La Recherche Aérospatiale, ONERA*, Vol. 1982-2, 1982, pp. 1–14.
- [15] Zagaynov, G. and Goman, M., “Bifurcation Analysis of Critical Aircraft Flight Regimes,” *14th Congress of the Int. Council of the Aeronautical Sciences (ICAS)*, Vol. 1, Toulouse, 1984, pp. 217–223, ICAS-84-4.2.1.
- [16] Jahnke, C. and Culick, F., “Application of bifurcation theory to the high-angle-of-attack dynamics of the F-14,” *J. Aircraft*, Vol. 31, No. 1, Jan.-Feb. 1994, pp. 26–34, DOI 10.2514/3.46451.
- [17] Avanzini, G. and de Matteis, G., “Bifurcation Analysis of a Highly Augmented Aircraft Model,” *J. Guidance, Control, and Dynamics*, Vol. 20, No. 4, July 1997, pp. 754–759, DOI 10.2514/2.4108.
- [18] Goman, M., Zagaynov, G., and Khramtsovsky, A., “Application of Bifurcation Methods to Nonlinear Flight Dynamics Problems,” *Prog. Aerospace Sci.*, Vol. 33, 1997, pp. 539–586, DOI 10.1016/S0376-0421(97)00001-8.
- [19] Planeaux, J., Beck, J., and Baumann, D., “Bifurcation Analysis of a Model Fighter Aircraft with Control Augmentation,” *AIAA Atmospheric Flight Mechanics Conference*, Portland, OR, August 1990, AIAA-90-2836, DOI 10.2514/6.1990-2836.
- [20] Littleboy, D. and Smith, P., “Bifurcation Analysis of a high Incidence Aircraft with Nonlinear Dynamic Inversion Control,” *AIAA Atmospheric Flight Mechanics Conference*, New Orleans, LA, August 1997, pp. 629–639, AIAA-97-3717-CP, DOI 10.2514/6.1997-3717.
- [21] Jones, C., Lowenberg, M., and Richardson, T., “Tailored Dynamic Gain-Scheduled Control,” *J. Guidance, Control, and Dynamics*, Vol. 29, No. 6, Nov.-Dec. 2006, pp. 1271–1281, DOI 10.2514/1.17295.

- [22] Kwatny, H., Dongmo, J.-E., Chang, B.-C., Bajpai, G., Yasar, M., and Belcastro, C., “Nonlinear Analysis of Aircraft Loss of Control,” *J. Guidance, Control, and Dynamics*, Vol. 36, No. 1, Jan.-Feb. 2013, pp. 149–162, DOI 10.2514/1.56948.
- [23] Goman, M. and Khrantsovsky, A., “Application of Continuation and Bifurcation Methods to the Design of Control Systems,” *Phil. Trans. R. Soc. Lond. A*, Vol. 356, No. 1745, 1998, pp. 2277–2295, DOI 10.1098/rsta.1998.0274.
- [24] Richardson, T., Lowenberg, M., di Bernardo, M., and Charles, G., “Design of a Gain-Scheduled Flight Control System Using Bifurcation Analysis,” *J. Guidance, Control, and Dynamics*, Vol. 29, No. 2, Mar.-Apr. 2006, pp. 444–453, DOI 10.2514/1.13902.
- [25] Crespo, L. G., Kenny, S. P., Cox, D. E., and Murri, D. G., “Analysis of Control Strategies for Aircraft Flight Upset Recovery,” *AIAA Guidance, Navigation, and Control Conference*, 2012, AIAA-2012-5026, DOI 10.2514/6.2012-5026.
- [26] Cunningham, K., Cox, D. E., Murri, D. G., and Riddick, S. E., “A Piloted Evaluation of Damage Accommodating Flight Control Using a Remotely Piloted Vehicle,” *AIAA Guidance Navigation and Control Conference, Portland, OR*, August 2011, AIAA-2011-6451, DOI 10.2514/6.2011-6451.
- [27] Murch, A. M., “A Flight Control System Architecture for the NASA AirSTAR Flight Test Infrastructure,” *AIAA Guidance Navigation and Control Conference, Honolulu, HI*, August 2008, AIAA-2008-6990, DOI 10.2514/6.2008-6990.
- [28] Rugh, W. J. and Shamma, J. S., “Research on Gain Scheduling,” *Automatica*, Vol. 36, No. 10, 2000, pp. 1401–1425, DOI 10.1016/S0005-1098(00)00058-3.
- [29] Carbaugh, D. and Rockliff, L., “The Airplane Upset Recovery Training Aid, Revision 2,” 2008, URL: <http://flightsafety.org/archives-and-resources/airplane-upset-recovery-training-aid> [cited 17 July 2014].
- [30] Lambregts, A. A., Nesemeier, G., Wilborn, J. E., and Newman, R. L., “Airplane Upsets: Old Problem, New Issues,” *AIAA Modeling and Simulation Technologies Conference and Exhibit*, 2008, AIAA-2008-6867, DOI 10.2514/6.2008-6867.
- [31] Doedel, E. J. and Oldeman Bart, E., “AUTO-07P: Continuation and Bifurcation Software for Ordinary Differential Equations,” Tech. rep., <http://sourceforge.net/projects/auto-07p/files/auto07p/> [retrieved 29 April 2013], Jan. 2012.
- [32] Coetzee, E., Krauskopf, B., and Lowenberg, M., “The Dynamical Systems Toolbox: Integrating AUTO into Matlab,” *16th US National Congress of Theoretical and Applied Mechanics*, No. USNCTAM2010-827, USNCTAM, Pennsylvania State University, PA, June-July 2010.
- [33] Cook, M. V., *Flight Dynamics Principles*, No. ISBN 0 340 63200 3, Arnold, 338 Euston Road, London, NW1 3BH, UK, 1997.
- [34] Cooper, G. E. and Harper Jr., R. P., “The use of Pilot Ratings in the Evaluation of Aircraft Handling Qualities,” Technical Note TN D-5153, NASA, 1969.
- [35] Gill, S. J., *Investigation into upset and upset recovery using bifurcation analysis*, PhD dissertation, Bristol University, Department of Aerospace Engineering, 2014, Submission under review.